Cosmic Ray Albedo Neutron Decay (CRAND) as a Source of Inner Belt Electrons: Energy Spectrum Study

K. Zhang, X. Li, H. Zhao, Q. Schiller, L. -Y. Khoo, Z. Xiang, R. Selesnick, M. A. Temerin, J. A. Sauvaud

Geophysical Research Letters

Key Points:
- CRAND-produced electrons are identified unequivocally by both CSSWE and DEMETER at the inner edge of the inner belt
- The electron source at low L, where no trapped electrons exist, is validated to be CRAND through a study of energy spectra
- During quiet times, CRAND is the dominant source of >250-keV quasitrapped electrons for the entire inner belt and slot region

Supporting Information:
- Supporting Information S1

Correspondence to:
K. Zhang,
kun.zhang@lasp.colorado.edu

Cosmic Ray Albedo Neutron Decay (CRAND) as a Source of Inner Belt Electrons: Energy Spectrum Study

K. Zhang[1,2], X. Li[1,2], H. Zhao[1], Q. Schiller[3], L.-Y. Khoo[1,2], Z. Xiang[1], R. Selesnick[4], M. A. Temerin[5], and J. A. Sauvaud[6]

[1]Laboratory for Atmospheric and Space Physics, University of Colorado Boulder, Boulder, CO, USA, [2]Department of Aerospace Engineering Sciences, University of Colorado Boulder, Boulder, CO, USA, [3]Heliophysics Laboratory, NASA Goddard Space Flight Center, Greenbelt, MD, USA, [4]Space Vehicles Directorate, Air Force Research Laboratory, Kirtland AFB, NM, USA, [5](formerly from) Space Sciences Laboratory, University of California, Berkeley, CA, USA, [6]Institut de Recherche en Astrophysique et Planétologie-IRAP, Université de Toulouse, CNRS, UPS, CNES, Toulouse, France

Abstract Cosmic Ray Albedo Neutron Decay (CRAND) has been recently confirmed as a source of energetic electrons at the inner edge of the inner belt by the Colorado Student Space Weather Experiment (CSSWE) mission. Here we use observations from the Detection of Electro-Magnetic Emissions Transmitted from Earthquake Regions (DEMETER) mission, to investigate the CRAND contribution to inner belt electrons quantitatively over a broad energy range (~100–800 keV). Spectral fitting analysis supports the conclusion that CRAND is the most important electron source at the inner edge of the inner belt. For the first time, we show that CRAND is the dominant source of >250-keV quasitrapped electrons throughout the inner belt and slot region during quiet times. We suggest that additional sources for <250-keV electrons exist, perhaps from inward transport. In contrast, dynamics of electrons in the inner belt and slot region is dominated by injections during active times.

Plain Language Summary Albedo neutrons are produced when cosmic ray particles (energetic protons and alpha particles) enter the Earth's atmosphere and then decay into protons, electrons, and antineutrinos, which is known as the Cosmic Ray Albedo Neutron Decay (CRAND) process. The produced energetic protons fill up the inner proton radiation belt, but the CRAND-produced electrons were not expected to be an important source of the electron belts until measurements from the Colorado Student Space Weather Experiment (CSSWE) mission recently showed that 500-keV electrons at the inner edge of the inner belt are produced by CRAND. This study uses measurements from the Detection of Electro-Magnetic Emissions Transmitted from Earthquake Regions (DEMETER) mission and analyze the electron energy spectrum over a broad energy range (~100–800 keV), combining the theoretical calculation of the energy spectrum of CRAND-produced electrons, to confirm CRAND is the dominant electron source at the inner edge of the inner belt. Furthermore, we show that CRAND is also an important source of >250-keV quasitrapped electrons (freshly produced ones) in the inner belt and slot region during quiet times. This study discusses the CRAND contribution to the radiation belt electrons and shows that with the knowledge of this new electron source, some other physics processes, such as pitch angle scattering, need to be revisited and quantified.

1. Introduction

The inner electron radiation belt is a relatively stable region where the electron intensity is typically subject to steady decay but increases occasionally during periods of extreme geomagnetic activity (e.g., Li et al., 2015; Selesnick, 2016; Zhao & Li, 2013). During large geomagnetic storms, injections dominate the dynamics of the inner belt electrons. It has been reported that injections may cause a significant enhancement in the 500-keV electron flux at about $L = 2$ and that the increase is observable down to $L = 1.25$ (Rosen & Sanders, 1971; L can be viewed as the geocentric distance in R_E at the magnetic equator if the Earth's magnetic field is approximated as a dipole). During geomagnetic quiet times, sources of inner belt electrons include inward radial diffusion (e.g., Cunningham et al., 2018; Selesnick, 2016) and CRAND, which was proposed at the dawn of the space age and recently confirmed by Li et al. (2017) based on observations from the Colorado Student Space Weather Experiment (CSSWE) at the inner edge of the inner belt. Meanwhile, important loss processes for inner belt electrons include pitch angle scattering, which precipitates electrons into the
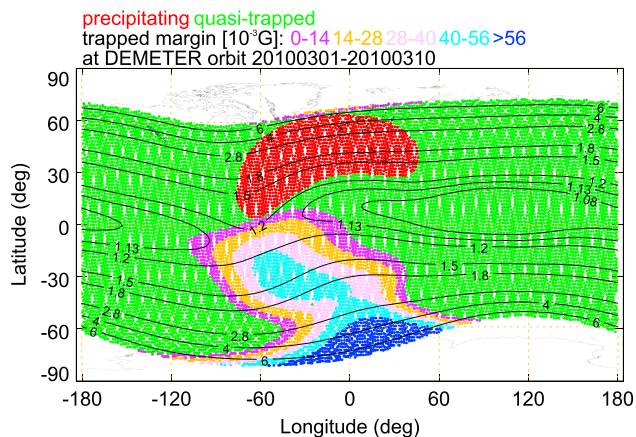
Figure 1. DEMETER orbit from March 1, 2010 to March 10, 2010 plotted over a map color-coded with the populations of the electrons mirroring at the satellite. *L* contours are overplotted as the black solid lines. Higher trapped margin means that electrons are more stably trapped. The detailed method and the definition of the trapped status margin are described in Selesnick (2015b).

atmosphere, and energy loss caused by collision, both controlling the lifetime of the electrons (Selesnick, 2012, 2016). Because Earth's magnetic field is shifted relative to its geographic center with local anomalies where the magnetic field strength is weak, such as the South Atlantic Anomaly (SAA) region (about −90° to 40° in longitude), some electrons will not precipitate until they drift to those regions. In this context, electrons can be categorized into three populations (Selesnick et al., 2004): (1) precipitating electrons with lifetime shorter than one bounce period, (2) quasitrapped electrons with lifetime longer than one bounce period but shorter than one drift period, and (3) stably trapped electrons with lifetime longer than one drift period.

Low Earth orbit (LEO) satellites with high inclinations are able to measure each of these three electron populations. As an example, Figure 1 shows the location (geographic latitude and longitude) of Detection of Electro-Magnetic Emissions Transmitted from Earthquake Regions (DEMETER; a LEO satellite) plotted on a map, with color representing the measured electron population assuming electrons are mirroring at the satellite location (the instrument points roughly in the perpendicular direction of the geomagnetic field allowing an ~20° variation; for the method of identifying the different populations, see Selesnick, 2015b). Note that the overplotted *L* contours and all *L* values presented later in this study is McIlwain *L* (McIlwain, 1961) calculated using the International Geomagnetic Reference Field (IGRF) model (Thébault et al., 2015). As shown in Figure 1, there are only quasitrapped electrons at about $L < 1.14$, which is at the inner edge of the inner belt. However, all three populations can be measured at higher *L*. Moreover, for a given *L*, the type of electron population sampled by the instrument is highly dependent on longitude, which can be used to study the dynamics of a specific electron population at LEO. For instance, Zhao and Li (2013) extracted the stably trapped electron fluxes from DEMETER data to investigate a slot region penetration event. Previous studies also used LEO measurements to study quasitrapped electrons (e.g., Li et al., 2015; Selesnick et al., 2003; Tu et al., 2010). Zhang et al. (2017) reported that the quasitrapped sub-MeV electrons exist in the inner belt, slot region, and the outer belt. The conventional understanding of the source of quasitrapped electrons has been the pitch angle scattering of stably trapped electrons, where the intensity could be explained by a balance between azimuthal drift and pitch angle scattering. Both theoretical calculation and simulation works have been conducted to evaluate the pitch angle diffusion coefficient and electron lifetime quantitatively (e.g., Abel & Thorne, 1999; Lyons et al., 1972; Pham et al., 2017; Schiller et al., 2017; Selesnick et al., 2003, 2004; Tu et al., 2010). Note that these studies only focused on the regions where stably trapped electrons are abundant.

Recently, however, Li et al. (2017) analyzed measurements from CSSWE, a LEO CubeSat, and found quasitrapped electrons of 500 keV at the inner edge of the inner radiation belt, indicating that a different source of these electrons is required rather than pitch angle scattering, since there are no stably trapped electrons at those *L* to be scattered. Li et al. (2017) further reported that the quasitrapped electron intensity below $L = 1.2$ is steady and not influenced by geomagnetic activity. They conclude that those electrons originate from CRAND, a relatively stable process. Neutrons are produced when cosmic ray particles, composed of GeV protons and alpha particles, interact with the neutral molecules/atoms in the Earth's atmosphere (Dunai, 2010). Neutrons have an average lifetime of 887 s and decay into protons, electrons, and antineutrinos. CRAND has been known as the source of the inner belt protons for decades (Singer, 1958) and was studied as a possible source of stably trapped electrons in the early days of the space age (Lenchek et al., 1961). For stably trapped radiation belt electrons, however, there are other stronger sources such as injection and plasma wave acceleration processes, so the CRAND contribution was not expected to be significant. As for quasitrapped electrons, though modeling and observations were done to study their behavior, early measurements are not sufficient to determine the CRAND contribution to the radiation belt electrons (e.g., Roederer et al., 1967). The recent findings of Li et al. (2017) show that CRAND-produced electrons are actually measurable in low *L* regions; however, their study only focused on one energy channel (500 keV). Here we combine satellite observations and theoretical calculations to discuss the CRAND contribution to
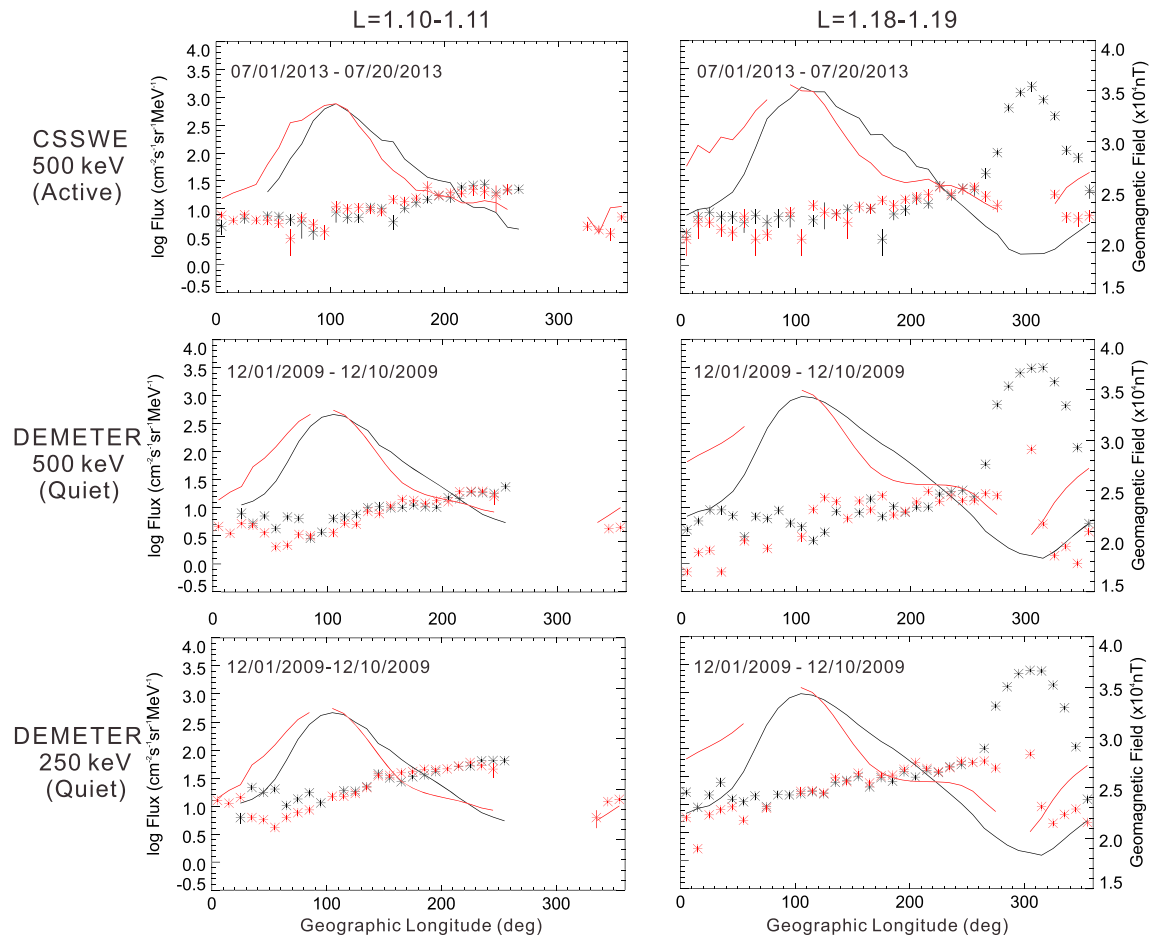
Figure 2. Electron fluxes (asterisks) as a function of geographic longitude at $L = 1.10$–1.11 and $L = 1.18$–1.19 from CSSWE and DEMETER measurements (note that the x axis range is different from Figure 1). Data are binned into 10° longitude bins and averaged over an active period for CSSWE and a quiet period for DEMETER. Solid lines are model geomagnetic field strength at satellite location. Black color stands for satellite locations in the Southern Hemisphere (in terms of geographic latitude) and red color in the north. Statistical error bars are in units of flux per square root of N (N is the number of data points of each asterisks) and are visible when N is small.

energetic electrons quantitatively through energy spectrum analysis over an energy range of ~100–800 keV and further show the importance of CRAND as a function of the radial distance from Earth.

2. Data and Method

2.1. Electron Measurements

DEMETER is in a sun-synchronous circular orbit of 710-km altitude and 98.3° inclination, and the Instrument for the Detection of Particle (IDP) onboard provides electron flux measurement from 70 keV to 2.4 MeV at a fine energy resolution (Sauvaud et al., 2006). In this study, we utilize routine mode data that have ~18-keV energy resolution and 4-s cadence. As discussed in Sauvaud et al. (2006), IDP has more accurate measurements below 800 keV, which makes it ideal for studying CRAND-produced electrons. Electron measurements from the Relativistic Electron and Proton Telescope integrated little experiment (REPTile) instrument (Schiller & Mahendrakumar, 2010) onboard CSSWE (480 km × 790 km, 65° inclination, see Li et al., 2012, 2013) are also used in this study.

Figure 2 shows CSSWE/REPTile and DEMETER/IDP observations as a function of geographic longitude, in L ranges of 1.10–1.11 and 1.18–1.19. CSSWE 500-keV electron fluxes are converted from count rates during an active period from 1 to 20 July 2013 when three moderate storms took place (see Extended Data Figure 2 in Li et al., 2017, for the conversion method). DEMETER electron fluxes at 250 and 500 keV are presented

during an extended quiet period from 1 to 10 December 2009, after *Dst* stayed above −50 nT for the previous 4 months. Data are binned into 10° longitude grids and averaged over a 20-day window for CSSWE and a 10-day window for DEMETER. Magnetic field strength at the satellite location is calculated using the IGRF model and overplotted against longitude (CSSWE altitude is assumed to be 640 km, which is its average altitude during this period, and actual altitude of DEMETER is used in the calculation). It should be noted that the peak stably trapped electron fluxes measured in the center of SAA by DEMETER (at ~310° longitude) at 250 and 500 keV are nearly identical, which could be associated with the penetrating proton contamination in the SAA. Since inner belt protons are highly constrained to the SAA region, electron measurements outside the SAA are not affected by these protons. Both CSSWE and DEMETER show a positive slope in the longitude range from 0° to ~270°, which is the direction of electron drift. From Figure 1, electrons measured in this longitude range are quasitrapped at both *L* values. Both spacecraft show that quasitrapped electrons exist and accumulate during their azimuthal drift. Comparing fluxes measured at different longitudes that have the same magnetic field, we notice that electron fluxes are higher at locations closer to the west of the SAA, which indicates that the increased fluxes are not caused by the modulation of the magnetic field. The characteristics and maximum fluxes of 500-keV electrons (at ~270° longitude) from CSSWE and DEMETER are about the same and do not vary with *L* even though these measurements are years apart and under different geomagnetic conditions, requiring a steady source of the quasitrapped electrons in near-Earth space, consistent with CRAND.

2.2. β-Decay Spectrum

Since some cosmic ray particles are extremely energetic, they can reach any latitude in low-altitude regions. Electrons, therefore, are produced by CRAND at all *L* values. At the inner edge of the inner belt, where electrons cannot be stably trapped, all CRAND-produced electrons are lost near the SAA. At larger *L*, however, CRAND contributes to both quasitrapped and stably trapped populations. Since neutron decay is well understood, its known properties enable evaluation of its contribution. In the neutron rest frame, electrons produced by neutron decay have a beta decay spectrum:

$$\psi(E) = C\sqrt{E(E + 2m_e c^2)}\left(E + m_e c^2\right)(Q - E)^2 \tag{1}$$

where E is electron kinetic energy, Q is the maximum available energy for electrons due to the mass difference ($Q = m_n c^2 - m_p c^2 - m_e c^2 = 782$ keV), and C is a constant ($C = 17.57$ MeV^{-5} when $\int \Psi dE = 1$; Selesnick, 2015a). Albedo neutrons below 1 eV have been determined to be responsible for the majority of the energetic electrons of interest (Hess et al., 1959; Lenchek et al., 1961). Therefore, we need only to consider neutrons at rest (also discussed in Hess et al., 1961, and Selesnick, 2015a). We can calculate the fluxes of the CRAND-produced electrons at different energies with lifetime τ_e (Li et al., 2017):

$$J(E) = n\frac{\tau_e}{\tau_n}\frac{v(E)\Psi(E)}{4\pi} \tag{2}$$

where J is the electron flux, n is the neutron density, τ_n is the neutron lifetime, and v is the electron velocity. As shown in Figure 2, J depends on the longitude, which determines the lifetime that electrons have survived (τ_e), but the longitude should not affect the neutron density theoretically. A reasonable estimate of the quasitrapped electron lifetime is a fraction of their drift period, τ_d. An approximation of τ_d for equatorial mirroring electrons from Roederer (1970) is as follows:

$$\tau_d \approx \frac{4\pi e B_E R_E^2}{3L m_0 c^2 \gamma\left(1 - \frac{1}{\gamma^2}\right)} \tag{3}$$

where e is the electron charge, m_0 is the electron rest mass, c is the speed of light, B_E is the geomagnetic field strength at the surface of Earth (3×10^{-5} T), R_E is the Earth radius, and γ is the Lorentz factor. Using equation (2), Li et al. (2017) calculated the neutron density in 2013 to be 2×10^{-9} cm^{-3} based on the 500-keV electron fluxes measured by CSSWE.

2.3. "Best-Fit" Method of Neutron Density Determination

To improve the accuracy in the determination of the neutron density, we utilize electron measurements from DEMETER at a series of energy channels instead of one single energy channel. Based on
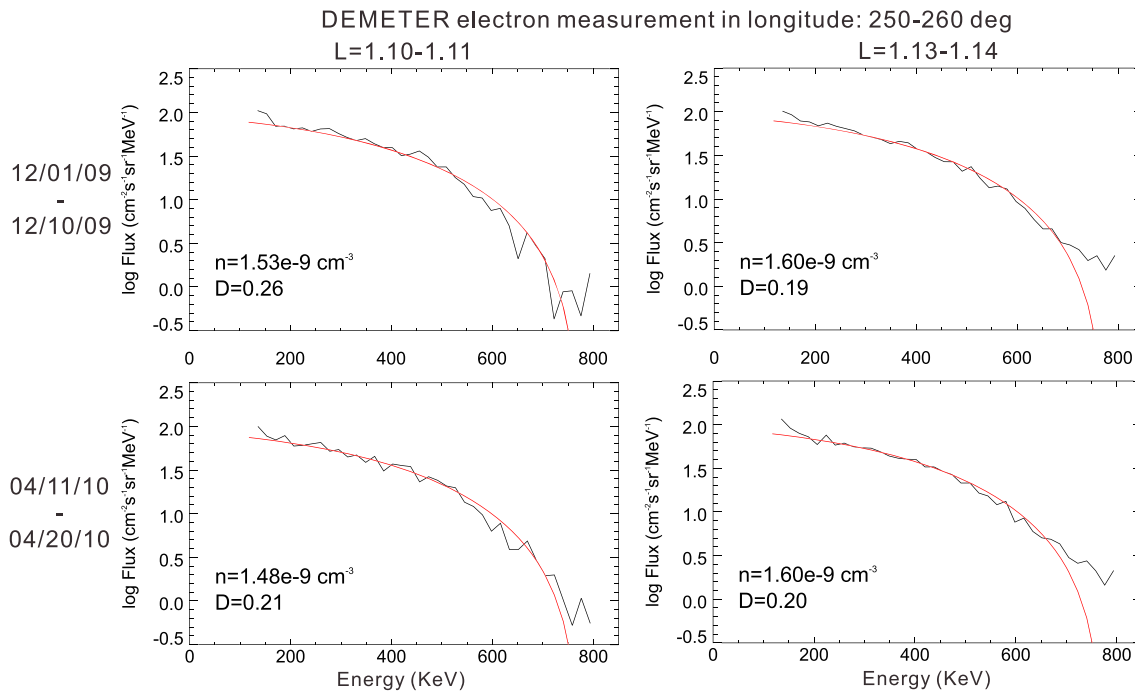
Figure 3. DEMETER electron energy spectrum (black) at the inner edge of the inner belt during 1–10 December 2009 (top) and 11–20 April 2010 (bottom), compared with the calculated electron flux (red) based on the beta decay spectrum and the "best-fit" neutron density (*n*), in the longitude range of 250°–260° and the *L* ranges of 1.10–1.11 (left column) and 1.13–1.14 (right column). *D* is the average normalized bias between calculated spectrum and measurements in the energy range of 126–785 keV.

equation (2), we can calculate the fluxes of the CRAND-produced electrons at different energies for a given *n*. Here we evaluate a goodness of fit between the calculated fluxes J_i (*i* is the *i*th energy channel) and DEMETER measured fluxes Jd_i by an average normalized bias defined as $D = \frac{\sum_i \frac{|Jd_i - J_i|}{Jd_i}}{m}$, where *m* is the number of energy channels. By adjusting *n*, a minimum *D* can be found, and we define this situation as the "best fit." In this way, we determine a "best-fit" *n*, which describes the ambient neutron density.

3. Energy Spectrum Observations

We select a quiet time period, 1–10 December 2009, and an active period, 11–20 April 2010, to calculate the neutron density and the energy spectrum of CRAND-produced electrons using DEMETER measurements at 250°–260° longitude at the inner edge of the inner belt (*L* = 1.10–1.11 and *L* = 1.13–1.14). Electrons at these *L* are all quasitrapped (see Figure 1 in Li et al., 2017). Assuming that these electrons have survived about 80% of their drift period, we apply the "best-fit" method described in section 2.3 to determine the neutron density. Using equation (3), we calculate the energy spectrum of CRAND-produced electrons, shown as the red lines in Figure 3, and then compare it with DEMETER measurements (black lines in Figure 3). For both periods and for both *L*, the maximum "best-fit" *D* of 126–785-keV electrons is 0.26, which means the average relative difference between calculated spectrum and measurements is within 26%. As a comparison, Whittaker et al. (2013) analyzed the energy resolution error of DEMETER electron measurements and showed that the maximum uncertainty due to energy error is about 13% for <800-keV electrons and 7% for <600-keV electrons. We argue that the actual flux uncertainty should be higher if other potential errors are taken into account. Moreover, since the measurement uncertainty is high at >600 keV, we further calculate the maximum *D* to be about 11% for 126–607-keV electrons. Since the maximum *D* of the fitting is comparable to the flux uncertainty, we argue that CRAND spectra fit well with the measured electron fluxes. Hence, we suggest that CRAND is the dominant electron source at the inner edge of the inner belt.

We also use energy spectra to investigate whether CRAND is the dominant source of quasitrapped electrons at higher *L* in the inner belt where stably trapped electrons exist. Figure 4 shows DEMETER measured
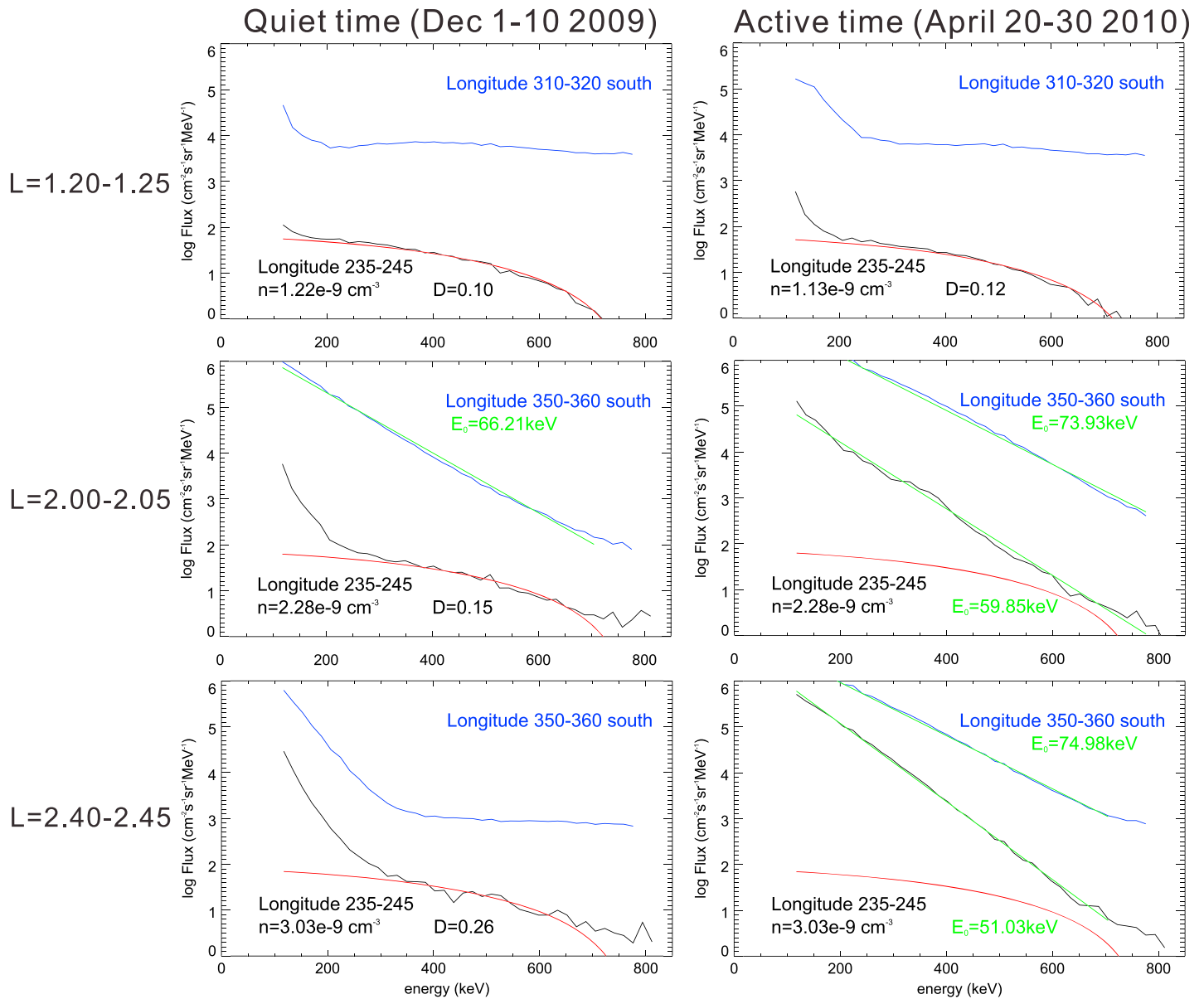
Figure 4. Electron energy spectra from DEMETER measurements at different *L* in 1–10 December 2009 (left column) and 20–30 April 2010 (right column). The period 1–10 December 2009 is an extended quiet time when the minimum *Dst* in the past 4 months is above −40 nT. The period 20–30 April 2010 is right after a magnetic storm with a minimum *Dst* of −81 nT. Black lines show the measured quasitrapped electron fluxes west of the SAA, and the blue lines show the stably trapped fluxes in the SAA. Red lines are calculated (CRAND) spectra (neutron density denoted as *n* in each panel). Green lines are fitted exponential spectra with E_0 noted in the figure. The definition of *D* is the same as Figure 3 except it is calculated only for quasitrapped electrons of 250–696 keV.

energy spectra of both quasitrapped (black lines) and stably trapped electrons (blue lines) at selected *L*. Quasitrapped electrons are selected from 235° to 245° in longitude, which is further from the SAA than the region used in Figure 3, to avoid any potential mixture with trapped electrons. Stably trapped electrons are selected from various longitude ranges based on Figure 1. We first investigate the extended quiet period, 1–10 December 2009 (left column). Comparing the spectra calculated based on the "best-fit" n (red lines) with the measured quasitrapped fluxes (black lines), we find that the average normalized bias, *D* in the "best-fit" case for 126–785-keV electrons is 0.18 at *L* = 1.2, which suggests a good fit, but at *L* > 2, *D* is greater than 0.4 since the measured <250-keV electron fluxes are significantly higher than the CRAND contribution, indicating additional sources of <250-keV electrons. For example, one potential

source process of these low-energy electrons is inward transport of outer belt electrons (e.g., Zhao & Li, 2013). Moreover, less reliable measurements at high energy also increase the uncertainty as we have discussed. We, therefore, limit the calculation to 250–696-keV electrons and then find $D \leq 0.26$, indicating CRAND is still the dominant source of >250-keV quasitrapped electrons in the inner belt and slot region ($L \sim 2.4$) during extended quiet time.

In addition to the quiet period, we present data in a period immediately following a magnetic storm with a minimum *Dst* of −81 nT, from 20 to 30 April 2010, when lower-energy electrons penetrated through the slot region (right column). The CRAND contribution to the quasitrapped electrons is only important at $L < 2$ ($D \sim 0.3$ in the "best-fit" case at $L = 1.9$–1.95 for 250–696-keV electrons). At $L = 2$ and $L = 2.4$, CRAND contributions (red lines), predicted based on the quiet time case since CRAND is not affected by geomagnetic activity, are significantly lower than the observed fluxes. The measured quasitrapped electron fluxes fit well with exponential spectra ($J = C \, \exp\left(-\frac{E}{E_0}\right)$, where C and E_0 are constant) shown as green lines. In some panels, stably trapped electron fluxes (blue lines) show an almost flat spectrum for higher energy electrons (e.g., >250-keV electrons at $L = 1.2$), possibly due to penetrating proton contamination. Rather than CRAND spectrum, the observed stably trapped electrons are more likely to have an exponential spectrum.

4. Discussion and Conclusions

The excellent agreement between energy spectra measured by DEMETER and the theoretical energy spectrum of CRAND-produced electrons confirms that CRAND is the dominant source of the quasitrapped electrons of energies up to ~800 keV at the inner edge of the inner belt in both quiet and active times. Furthermore, in quiet times, the CRAND contribution is significant for >250-keV electrons throughout the inner belt and slot region. In active times, however, the inner belt and slot region at $L > 2$ is dominated by injections, and the contribution from CRAND is negligible. Moreover, we report higher calculated neutron density at larger L or higher magnetic latitude (at fixed altitude and up to $L = 2.4$), which is consistent with the geomagnetic shielding effect that gives cosmic rays more access to higher magnetic latitude regions, as discussed by Hess et al. (1961). The neutron density calculation in this study is only a simplified model, and we suggest that a more detailed work is needed to estimate the neutron density accurately.

At larger L in the inner belt, two different populations of quasitrapped electrons are observed during the quiet period: <250-keV electrons with an exponential spectrum and >250-keV electrons with a CRAND spectrum. During both quiet and active times, the quasitrapped electron fluxes at <250 keV are higher than the calculation. For example, comparing the calculated flux of CRAND-produced electrons (red lines in Figure 4) to the measured electron flux (black lines), we estimate that at $L = 2.4$ CRAND only contributes about 10% of the quasitrapped 200-keV electrons during quiet times and that during active times this number further decreases to about 0.45%, indicating a much stronger source of low-energy electrons. Note that the <250-keV quasitrapped electrons tend to have similar energy spectra to stably trapped electrons, while the >250-keV electrons have totally different spectra from the stably trapped electrons. On one hand, lower-energy electrons are more easily transported into the inner belt from the outer regions by injections or diffusion (Reeves et al., 2016), so the energy spectra of both quasitrapped and stably trapped electrons below 250 keV are likely to be dominated by inward transport processes and differ from the CRAND spectrum. On the other hand, it is possible that the <250-keV quasitrapped electrons have similar energy spectra to trapped electrons because they are scattered into the drift loss cone from the stably trapped population. The modeled results by Selesnick (2012) indicate that collision-induced pitch angle scattering from stably trapped electrons could be an effective source of the 200-keV quasitrapped electrons at $L = 1.3$. The results of the same simulation for 500-keV electrons using pitch angle scattering, however, do not explain the observed quasitrapped electrons. Here we suggest that these 500-keV quasitrapped electrons are likely produced by CRAND and therefore unrelated to most of the stably trapped population (for electron observations at different L and energy by DEMETER, see the supporting information).

In the inner belt, CRAND as a newly identified important electron source may affect conclusions of other physics problems. For example, without the knowledge of the CRAND-produced electrons, previous studies may have overestimated the pitch angle scattering rate and diffusion coefficient to some extent, especially in the inner belt. Since the CRAND process is relatively uniform in space, in principle such electrons also exist

at larger *L* in the outer belt. The outer belt, however, is highly dynamic, and the electron fluxes are much larger than CRAND production, so the CRAND contribution is negligible. For example, during active times, at *L* ~ 2 and *L* ~ 2.4, both quasitrapped and stably trapped electrons fit exponential spectra well. In this case, quasitrapped electrons could be produced by enhanced pitch angle scattering from the stably trapped population, as their energy spectra are similar. Moreover, stably trapped electrons have harder spectra than quasitrapped electrons, which indicates that the pitch angle scattering process is possibly more efficient at lower energies.

In summary, using DEMETER electron flux measurements with fine-energy resolutions, we have studied energy spectra of inner belt electrons and focus on their connection with CRAND-produced electrons. Here we conclude the following:

1. DEMETER and CSSWE both identified CRAND-produced electrons at the inner edge of the inner belt.
2. At *L* < 1.14 where no stably trapped electrons exist, the electron energy spectrum matches the beta decay spectrum almost perfectly, confirming that CRAND is the dominant source of these electrons.
3. During quiet times, CRAND is an important source of >250-keV quasitrapped electrons in the inner belt and slot region based on spectral fits to the CRAND spectra. Possible sources for <250-keV quasitrapped electrons include inward transport processes and more efficient pitch angle scattering.
4. During active times, injections dominate the dynamics of electrons in the inner belt and slot region, and the CRAND contribution is insignificant.

References

Abel, B., & Thorne, R. M. (1999). Modeling energetic electron precipitation near the South Atlantic anomaly. *Journal of Geophysical Research*, *104*(A4), 7037–7044. https://doi.org/10.1029/1999JA900023

Cunningham, G. S., Loridan, V., Ripoll, J.-F., & Schulz, M. (2018). Neoclassical diffusion of radiation-belt electrons across very low *L*-shells. *Journal of Geophysical Research: Space Physics*, *123*, 2884–2901. https://doi.org/10.1002/2017JA024931

Dunai, T. J. (2010). Origin and nature of cosmic rays. In *Cosmogenic nuclides: Principles, concepts and applications in the Earth surface sciences* (p. 3). Cambridge, UK: Cambridge University Press. https://doi.org/10.1017/CBO9780511804519.002

Hess, W. N., Canfield, E. H., & Lingenfelter, R. E. (1961). Cosmic-ray neutron demography. *Journal of Geophysical Research*, *66*(3), 665–677. https://doi.org/10.1029/JZ066i003p00665

Hess, W. N., Patterson, H. W., Wallace, R., & Chupp, E. L. (1959). Cosmic-ray neutron energy spectrum. *Physical Review*, *116*(2), 445–457. https://doi.org/10.1103/PhysRev.116.445

Lenchek, A., Singer, S., & Wentworth, R. (1961). Geomagnetically trapped electrons from cosmic ray albedo neutrons. *Journal of Geophysical Research*, *66*(12), 4027–4046. https://doi.org/10.1029/JZ066i012p04027.

Li, X., Palo, S., Kohnert, R., Gerhardt, D., Blum, L., Schiller, Q., et al. (2012). Colorado student space weather experiment: Differential flux measurements of energetic particles in a highly inclined low Earth orbit. In D. Summers (Ed.), *Dynamics of the Earth's radiation belts and inner magnetosphere, Geophys. Monogr. Ser.* (Vol. 199, pp. 385–404). Washington, DC: American Geophysical Union. https://doi.org/10.1029/2012GM001313

Li, X., Schiller, Q., Blum, L., Califf, S., Zhao, H., Tu, W., et al. (2013). First results from CSSWE CubeSat: Characteristics of relativistic electrons in the near-Earth environment during the October 2012 magnetic storms. *Journal of Geophysical Research: Space Physics*, *118*, 6489–6499. https://doi.org/10.1002/2013JA019342

Li, X., Selesnick, R., Schiller, Q., Zhang, K., Zhao, H., Baker, D. N., & Temerin, M. A. (2017). Measurement of electrons from albedo neutron decay and neutron density in near-Earth space. *Nature*, *552*(7685), 382. https://doi.org/10.1038/nature24642–385.

Li, X., Selesnick, R. S., Baker, D. N., Jaynes, A. N., Kanekal, S. G., Schiller, Q., et al. (2015). Upper limit on the inner radiation belt MeV electron intensity. *Journal of Geophysical Research: Space Physics*, *120*, 1215–1228. https://doi.org/10.1002/2014JA020777

Lyons, L. R., Thorne, R. M., & Kennel, C. F. (1972). Pitch-angle diffusion of radiation belt electrons within the plasmasphere. *Journal of Geophysical Research*, *77*(19), 3455–3474. https://doi.org/10.1029/JA077i019p03455

McIlwain, C. E. (1961). Coordinates for mapping the distribution of magnetically trapped particles. *Journal of Geophysical Research*, *66*(11), 3681–3691. https://doi.org/10.1029/JZ066i011p03681

Pham, K. H., Tu, W., & Xiang, Z. (2017). Quantifying the precipitation loss of radiation belt electrons during a rapid dropout event. *Journal of Geophysical Research: Space Physics*, *122*, 10,287–10,303. https://doi.org/10.1002/2017JA024519

Reeves, G. D., Friedel, R. H. W., Larsen, B. A., Skoug, R. M., Funsten, H. O., Claudepierre, S. G., et al. (2016). Energy-dependent dynamics of keV to MeV electrons in the inner zone, outer zone, and slot regions. *Journal of Geophysical Research: Space Physics*, *121*, 397–412. https://doi.org/10.1002/2015JA021569

Roederer, J. G. (1970). Bounce motion, the second adiabatic invariant and drift shells. In *Dynamics of geomagnetically trapped radiation* (p. 57). New York: Springer. https://doi.org/10.1007/978-3-642-49300-3_2

Roederer, J. G., Welch, J. A., & Herod, J. V. (1967). Longitude dependence of geomagnetically trapped electrons. *Journal of Geophysical Research*, *72*(17), 4431–4447. https://doi.org/10.1029/JZ072i017p04431

Rosen, A., & Sanders, N. L. (1971). Loss and replenishment of electrons in the inner radiation zone during 1965–1967. *Journal of Geophysical Research*, *76*(1), 110–121. https://doi.org/10.1029/JA076i001p00110

Sauvaud, J. A., Moreau, T., Maggiolo, R., Treilhou, J. P., Jacquey, C., Cros, A., et al. (2006). High-energy electron detection onboard DEMETER: The IDP spectrometer, description and first results on the inner belt. *Planetary and Space Science*, *54*(5), 502–511. https://doi.org/10.1016/j.pss.2005.10.019

Schiller, Q., & Mahendrakumar, A. (2010). REPTile: A miniaturized detector for a CubeSat mission to measure relativistic particles in near-Earth space, Proceedings of the 24th Annual AIAA/USU Conference on Small Satellites, Frank J. Redd Student Scholarship Competition, SSC10-VIII-1.

Schiller, Q., Tu, W., Ali, A. F., Li, X., Godinez, H. C., Turner, D. L., et al. (2017). Simultaneous event-specific estimates of transport, loss, and source rates for relativistic outer radiation belt electrons. *Journal of Geophysical Research: Space Physics*, *122*, 3354–3373. https://doi.org/10.1002/2016JA023093

Selesnick, R. S. (2012). Atmospheric scattering and decay of inner radiation belt electrons. *Journal of Geophysical Research*, *117*, A08218. https://doi.org/10.1029/2012JA017793

Selesnick, R. S. (2015a). High-energy radiation belt electrons from CRAND. *Journal of Geophysical Research: Space Physics*, *120*, 2912–2917. https://doi.org/10.1002/2014JA020963

Selesnick, R. S. (2015b). Measurement of inner radiation belt electrons with kinetic energy above 1 MeV. *Journal of Geophysical Research: Space Physics*, *120*, 8339–8349. https://doi.org/10.1002/2015JA021387

Selesnick, R. S. (2016). Stochastic simulation of inner radiation belt electron decay by atmospheric scattering. *Journal of Geophysical Research: Space Physics*, *121*, 1249–1262. https://doi.org/10.1002/2015JA022180

Selesnick, R. S., Blake, J. B., & Mewaldt, R. A. (2003). Atmospheric losses of radiation belt electrons. *Journal of Geophysical Research*, *108*(A12), 1468. https://doi.org/10.1029/2003JA010160

Selesnick, R. S., Looper, M. D., & Albert, J. M. (2004). Low-altitude distribution of radiation belt electrons. *Journal of Geophysical Research*, *109*, A11209. https://doi.org/10.1029/2004JA010611

Singer, S. F. (1958). "Radiation Belt" and trapped cosmic-ray albedo. *Physical Review Letters*, *1*(5), 171–173. https://doi.org/10.1103/PhysRevLett.1.171

Thébault, E., Finlay, C. C., Beggan, C. D., Alken, P., Aubert, J., Barrois, O., et al. (2015). International geomagnetic reference field: The 12th generation. *Earth, Planets and Space*, *67*(1), 79. https://doi.org/10.1186/s40623-015-0228-9

Tu, W., Selesnick, R., Li, X., & Looper, M. (2010). Quantification of the precipitation loss of radiation belt electrons observed by SAMPEX. *Journal of Geophysical Research*, *115*, A07210. https://doi.org/10.1029/2009JA014949

Whittaker, I. C., Gamble, R. J., Rodger, C. J., Clilverd, M. A., & Sauvaud, J. A. (2013). Determining the spectra of radiation belt electron losses: Fitting DEMETER electron flux observations for typical and storm times. *Journal of Geophysical Research: Space Physics*, *118*, 7611–7623. https://doi.org/10.1002/2013JA019228

Zhang, K., Li, X., Schiller, Q., Gerhardt, D., Zhao, H., & Millan, R. (2017). Detailed characteristics of radiation belt electrons revealed by CSSWE/REPTile measurements: Geomagnetic activity response and precipitation observation. *Journal of Geophysical Research: Space Physics*, *122*, 8434–8445. https://doi.org/10.1002/2017JA024309

Zhao, H., & Li, X. (2013). Modeling energetic electron penetration into the slot region and inner radiation belt. *Journal of Geophysical Research: Space Physics*, *118*, 6936–6945. https://doi.org/10.1002/2013JA019240